Journal of Computational Physics 228 (2009) 147–157

Contents lists available at ScienceDirect

Journal of Computational Physics

journal homepage: www.elsevier.com/locate/jcp

Lattice Boltzmann modeling of microchannel flow in slip flow regime

Frederik Verhaeghe [a], Li-Shi Luo [b,*], Bart Blanpain [a]

[a] Department of Metallurgy and Materials Engineering, Katholieke Universiteit Leuven, Belgium
[b] Department of Mathematics and Statistics and Center for Computational Sciences, Old Dominion University, Norfolk, VA 23529, USA

ARTICLE INFO

Article history:
Received 23 January 2008
Received in revised form 2 September 2008
Accepted 2 September 2008
Available online 12 September 2008

Keywords:
Gas flow through microchannel
Slip flow
Lattice Boltzmann equation with multiple relaxation times

ABSTRACT

We present the lattice Boltzmann equation (LBE) with multiple relaxation times (MRT) to simulate pressure-driven gaseous flow in a long microchannel. We obtain analytic solutions of the MRT-LBE with various boundary conditions for the incompressible Poiseuille flow with its walls aligned with a lattice axis. The analytical solutions are used to realize the Dirichlet boundary conditions in the LBE. We use the first-order slip boundary conditions at the walls and consistent pressure boundary conditions at both ends of the long microchannel. We validate the LBE results using the compressible Navier–Stokes (NS) equations with a first-order slip velocity, the information-preservation direct simulation Monte Carlo (IP-DSMC) and DSMC methods. As expected, the LBE results agree very well with IP-DSMC and DSMC results in the slip velocity regime, but deviate significantly from IP-DSMC and DSMC results in the transition-flow regime in part due to the inadequacy of the slip velocity model, while still agreeing very well with the slip NS results. Possible extensions of the LBE for transition flows are discussed.

1. Introduction

The rapidly growing interest in micro-electro-mechanical systems (MEMS) has also stimulated a great interest in modeling and simulation methods for microflows [1,2]. In particular, the gaseous flow through a long microchannel has become an important test case for various numerical methods, because of its important applications in microdevices [2]. The physics of this flow has been well studied by now [2–4]. Even at very low Mach number, gaseous flows are often compressible in microdevices because of substantial pressure drops and density variations caused by viscous effects. In a long, constant-area microchannel, the degree of rarefaction and the Mach number increase along the channel, thus all Knudsen number regimes may be encountered, and the pressure drop becomes nonlinear. In essence, compressibility and rarefaction are the key characteristics of gaseous flows through a long microchannel [3].

Among various methods, the lattice Boltzmann equation (LBE) has been advocated as an effective means for microflows simulations because of its kinetic origin [5–20]. Based on a theoretical analysis and numerical evidence, we justify the application of the LBE method for simulation of microflows in the slip flow regime. We will focus our effort on pressure-driven flows through a long microchannel.

Numerous LBE studies have been devoted to pressure-driven microchannel flows [5–20]. Several interesting observations can be made. First of all, the lattice Bhatnagar-Gross-Krook (LBGK) model [22,21] is exclusively used in these works, although it is well known that the boundary conditions in the LBGK models depend on the viscosity [23,24] and that the so-called "slip velocity" observed in the LBGK models with bounce-back boundary conditions is a numerical artifact [25]. Second, regardless

* Corresponding author. Tel.: +1 757 683 5295; fax: +1 757 683 3885.
E-mail addresses: frederik.verhaeghe@mtm.kuleuven.be (F. Verhaeghe), lluo@odu.edu (L.-S. Luo).
URL: http://www.lions.odu.edu/~lluo (L.-S. Luo).

0021-9991/$ - see front matter © 2008 Elsevier Inc. All rights reserved.
doi:10.1016/j.jcp.2008.09.004

of the value of the Knudsen number Kn, the profile of the streamwise velocity u is a linear superposition of a *perfect* parabola and a constant slip velocity U_s at boundaries, and the magnitude of U_s depends on Kn. This is inconsistent with the solutions of the full or linearized Boltzmann equations. It is thus no surprise that the LBGK model yields *qualitatively* incorrect results [5] for microchannel flow at the Knudsen number $Kn = 0.194$ [26]. Because numerical analysis and convergence studies have not been shown in the LBE studies [5–20], nor have sufficient validation and verification been carried out, the validity of the LBE microflow modeling is in question [26].

In this work we intend to demonstrate the capability of the LBE method for microflow simulations. Through both theoretical analysis and numerical simulation, we will show that the LBE method can simulate microchannel flow. In particular, we obtain the analytic solutions of the LBE with various fluid–solid boundary conditions for the incompressible Poiseuille flow with its walls parallel to a lattice axis. Our analysis elucidates that the erroneous results in the previous LBE simulations are mostly due to the deficiencies in the LBGK model coupled with the bounce-back boundary conditions [25,24]. We will demonstrate that the LBE models with multiple relaxation times (MRT) [27–29] can overcome certain inconsistencies in the LBGK models with bounce-back boundary conditions. Although the present study only deals with the simple case of the two-dimensional Poiseuille flow with its walls aligned with a lattice axis, the boundary conditions for geometries with arbitrary curvatures have been proposed [31,23,24,30].

The remaining part of this paper includes a summary of known results for gaseous microchannel flow in Section 2; a brief exposition of the LBE method in Section 3; the analytic solutions of the LBE for the Poiseuille flow with various boundary conditions in Section 4; a description of boundary conditions used in the LBE simulations in Section 5; the numerical results for microchannel flow, compared with the slip Navier–Stokes solution, the DSMC and IP-DSMC data up to $Kn = 0.388$ in Section 6; and a concluding discussion in Section 7.

2. Theory of pressure-driven flow through a long microchannel

The two-dimensional isothermal flow through microchannels with low Mach number can be analyzed by using the Navier–Stokes equations [3,2]. A succinct summary of the known results relevant to the present work is provided below. For a long channel with a height H and length $L \gg H$, the flow variables can be represented as perturbation series of the aspect ratio

$$\varepsilon := H/L \ll 1. \tag{1}$$

The dimensionless parameters in the flow are the Reynolds number Re, the Mach number Ma and the Knudsen number Kn, all defined by the outlet flow conditions:

$$Re = \frac{\bar{\rho}_{\text{out}}\bar{u}_{\text{out}}H}{\mu}, \quad Ma = \frac{\bar{u}_{\text{out}}}{\sqrt{\gamma RT}}, \quad Kn = \sqrt{\frac{\pi\gamma}{2}}\frac{Ma}{Re}, \tag{2}$$

where $\bar{\rho}_{\text{out}}$ and $\bar{u}_{\text{out}}$ are the averaged density and the averaged streamwise velocity at the outlet, μ is the dynamic viscosity, γ is the heat capacity ratio, and R and T are the gas constant and temperature. The equation of state for an ideal gas, $p = \rho RT$, is also used in the analysis. It is assumed that $Ma = \mathrm{O}(\varepsilon^{\alpha})$ and $Re = \mathrm{O}(\varepsilon)$ for $0 < \alpha \leqslant 1$, thus $Kn = \mathrm{O}(\epsilon^{1-\alpha})$.

The boundary conditions are: at the walls, the spanwise velocity v vanishes and the streamwise velocity u is given by a first-order slip velocity model [32]:

$$u|_{\text{wall}} = \sigma Kn H \partial_y u|_{\text{wall}}, \qquad \sigma := (2 - \sigma_v)/\sigma_v, \tag{3}$$

where $\sigma_v \in (0, 1]$ is the tangential momentum accommodation coefficient, which is assumed to be 1 in the present study. The *averaged* pressures at the inlet and outlet are $\bar{p}_{\text{in}}$ and $\bar{p}_{\text{out}}$. With these boundary conditions, the time-independent solutions of the Navier–Stokes equations in the leading orders of ε are:

$$\tilde{p}(\tilde{x}) = \sqrt{(6\sigma Kn)^2 + (1 + 12\sigma Kn)\tilde{x} + \vartheta_p(\vartheta_p + 12\sigma Kn)(1 - \tilde{x})} - 6\sigma Kn, \tag{4a}$$

$$\tilde{u}(\tilde{x}, \tilde{y}) = -\frac{\varepsilon Re}{8\gamma Ma^2}\tilde{p}'\left(1 - 4\tilde{y}^2 + 4\sigma\frac{Kn}{\tilde{p}}\right), \tag{4b}$$

$$\tilde{v}(\tilde{x}, \tilde{y}) = \frac{\varepsilon^2 Re}{8\gamma Ma^2}\frac{1}{\tilde{p}}\left[\frac{1}{2}(\tilde{p}^2)''\left(1 - \frac{4}{3}\tilde{y}^2\right) + 4\sigma Kn\tilde{p}''\right]\tilde{y}, \tag{4c}$$

where $\vartheta_p = \bar{p}_{\text{in}}/\bar{p}_{\text{out}} = \bar{\rho}_{\text{in}}/\bar{\rho}_{\text{out}} > 1$, $\tilde{p}' := \mathrm{d}\tilde{p}/\mathrm{d}\tilde{x}$, $\tilde{p}'' := \mathrm{d}^2\tilde{p}/\mathrm{d}\tilde{x}^2$, $(\tilde{p}^2)'' := \mathrm{d}^2(\tilde{p}^2)/\mathrm{d}\tilde{x}^2$; and $\tilde{p} := p/p_{\text{out}}$, $\tilde{u} := u/\bar{u}_{\text{out}}$ and $\tilde{v} := v/\bar{u}_{\text{out}}$ are normalized quantities, and $\tilde{x} := x/L \in [0, 1]$ and $\tilde{y} := y/H \in [-1/2, +1/2]$. Based on Eq. (4a), it is understood that $\tilde{p} = \mathrm{O}(1)$, $\tilde{u} = \mathrm{O}(\varepsilon)$, $\tilde{v} = \mathrm{O}(\varepsilon^2)$ and that the dynamic viscosity $\mu = \rho v$ is a constant in the system [3].

Assuming $\rho = \bar{\rho}_{\text{out}}$ and integrating $\rho_{\text{out}}\tilde{u}(\tilde{x}, \tilde{y})$ at the outlet ($\tilde{x} = 1$) along the y direction, we obtain the total mass-flow rate:

$$\dot{m} = \frac{H^3 p_{\text{out}}^2}{24\mu LRT}(\vartheta_p - 1)(1 + \vartheta_p + 12\sigma Kn). \tag{5}$$

If $Kn = 0$, $\dot{m}$ reduces to $\dot{m}_{NS}$ for the no-slip Navier–Stokes flow,

$$\dot{m}_{NS} := \frac{H^3 p_{out}^2}{24\mu LRT}(\vartheta_p - 1)(1 + \vartheta_p),$$

and Eq. (5) can be rewritten as

$$\frac{\dot{m}}{\dot{m}_{NS}} = 1 + \frac{12\sigma Kn}{1 + \vartheta_p} \geqslant 1. \tag{6}$$

Clearly, the mass-flow rate $\dot{m}$ is enhanced in the slip flow.

The solutions given in Eqs. (4) can differ significantly from the no-slip Navier–Stokes solutions when $Kn > 0$. In addition to a constant slip component in the streamwise velocity u in proportion to Kn, the spanwise velocity v is non-zero. Also, the pressure along the channel center deviates from the linear distribution typical for the incompressible channel flow. These distinctive features of slip flows in a long microchannel have been verified experimentally and validated numerically [3,2]. The solutions only include first-order corrections in Kn, therefore they are not accurate for flows beyond the slip flow regime, for which more sophisticated models or Boltzmann equation have to be used [2].

3. Lattice Boltzmann equation with multiple relaxation times

The lattice Boltzmann equation (LBE) is a simple explicit algorithm, which can be derived from the linearized Boltzmann equation, and is often associated with a square or cubic lattice, $\boldsymbol{r}_j \in \mathbb{Z}^D$, on which the discretized single particle distribution function $f_i(\boldsymbol{r}_j, t_n) := f(\boldsymbol{r}_j, \boldsymbol{c}_i, t_n)$ evolves. The particle velocity space $\boldsymbol{\xi}$ is discretized into a symmetric discrete velocity set $\{\boldsymbol{c}_i\} = -\{\boldsymbol{c}_i\}$ so that in discrete time $t_n := \delta_t \mathbb{N}_0 = \delta_t\{0, 1, 2, \ldots\}$, fictitious particles represented by $\{f_i\}$ move synchronously from one grid point $\boldsymbol{r}_j$ to one of its neighbors $\boldsymbol{r}_j + \boldsymbol{c}_i\delta_t$ according to their discrete velocities. In the most general form, the lattice Boltzmann equation can be written as the following:

$$\mathbf{f}(\boldsymbol{r}_j + \boldsymbol{c}\delta_t, t + \delta_t) = \mathbf{f}(\boldsymbol{r}_j, t) + \boldsymbol{\Omega}[\mathbf{f}(\boldsymbol{r}_j, t)] + \mathbf{F}(\boldsymbol{r}_j, t), \tag{7}$$

where $\boldsymbol{\Omega}$ is the collision term and $\mathbf{F}$ is the external forcing, and the bold-face symbols denote $(Q{+}1)$-tuple vectors for a model of $(Q{+}1)$ discrete velocities, e.g.

$$\mathbf{f}(\boldsymbol{r}_j + \boldsymbol{c}\delta_t, t_n + \delta_t) = (f_0(\boldsymbol{r}_j, t_n + \delta_t), \ldots, f_Q(\boldsymbol{r}_j + \boldsymbol{c}_Q\delta_t, t_n + \delta_t))^{\mathsf{T}},$$

where T denotes the transpose operator, and the components of $\mathbf{F}$ are given by:

$$F_i = w_i\rho\frac{\boldsymbol{c}_i \cdot \boldsymbol{a}}{c_s^2}\delta_t, \tag{8}$$

where, ρ is the mass density, $\boldsymbol{a}$ is the acceleration due to an external force, and the values of the speed of sound c_s and the coefficients $\{w_i\}$ depend on the discrete velocity set $\{\boldsymbol{c}_i\}$.

The collision operator in the LBE method is modeled by a linear relaxation process with multiple relaxation parameters, which is carried out in the moment space as first proposed by d'Humières [27]:

$$\boldsymbol{\Omega} = -\mathsf{M}^{-1} \cdot \mathsf{S} \cdot [\mathbf{m} - \mathbf{m}^{(eq)}], \quad \mathbf{m} = \mathsf{M} \cdot \mathbf{f}, \quad \mathbf{f} = \mathsf{M}^{-1} \cdot \mathbf{m}, \tag{9}$$

where $\mathbf{m}$ and $\mathbf{m}^{(eq)}$ are moments and their equilibria, respectively, S is a positive-definite diagonal matrix of relaxation rates $\{s_i | i = 1, 2, \ldots, Q+1\}$:

$$\mathsf{S} = \mathrm{diag}(s_1, s_2, \ldots, s_{Q+1}), \qquad s_i \in (0, 2),$$

and M is the transformation matrix mapping the distribution functions to their moments,

$$\mathbf{m} = \mathsf{M} \cdot \mathbf{f}, \qquad \mathbf{f} = \mathsf{M}^{-1} \cdot \mathbf{m}.$$

In the present work, we will use the 9-velocity model on a square lattice in two dimensions (the D2Q9 model). The discrete velocity set $\{\boldsymbol{c}_i | i = 0, 1, \ldots, 8\}$ includes $\boldsymbol{c}_0 = (0, 0)$, $\boldsymbol{c}_1 = (1, 0)c = -\boldsymbol{c}_3$, $\boldsymbol{c}_2 = (0, 1)c = -\boldsymbol{c}_4$, $\boldsymbol{c}_5 = (1, 1)c = -\boldsymbol{c}_7$, and $\boldsymbol{c}_6 = (-1, 1)c = -\boldsymbol{c}_8$, where $c := \delta_x/\delta_t$. The values of the weight coefficients w_i are: $w_0 = 4/9$, $w_{1,2,3,4} = 1/9$, and $w_{5,6,7,8} = 1/36$. The equilibria of the moments are

$$m_1^{(eq)} = \rho, \quad m_2^{(eq)} = \rho(3\boldsymbol{u} \cdot \boldsymbol{u} - 2), \quad m_3^{(eq)} = \rho(1 - 3\boldsymbol{u} \cdot \boldsymbol{u}), \tag{10a}$$

$$m_{4,6}^{(eq)} = \rho(u, v) = -m_{5,7}^{(eq)}, \quad m_{5,7}^{(eq)} = -\rho(u, v), \tag{10b}$$

$$m_8^{(eq)} = \rho(u^2 - v^2), \quad m_9^{(eq)} = \rho uv, \tag{10c}$$

where ρ is the density, and $\boldsymbol{j} := \rho\boldsymbol{u} := \rho(u, v)$ is the flow momentum, and they are the conserved moments of the distribution functions for athermal fluids:

$$\rho = \sum_i f_i, \qquad \boldsymbol{j} = \sum_i \boldsymbol{c}_i f_i = \rho\boldsymbol{u}. \tag{11}$$

It can be shown that in this model, the kinematic viscosity v and the bulk viscosity ζ are given by:

$$v = \frac{1}{3}\left(\frac{1}{s_v} - \frac{1}{2}\right)c\delta_x, \tag{12a}$$

$$\zeta = \frac{1}{6}\left(\frac{1}{s_e} - \frac{1}{2}\right)c\delta_x, \tag{12b}$$

where $s_v = s_8 = s_9$ is the relaxation rate for the moments related to the stresses, and $s_q = s_2$ is the relaxation rate for the moment related to the energy; and the speed of sound is given by

$$c_s = \frac{1}{\sqrt{3}}c. \tag{13}$$

This MRT-LBE model reduces to the lattice BGK model [22,21] if $s_i = 1/\tau\ \forall i$. The matrix M and further details of this LBE model can be found in the paper by Lallemand and Luo [29].

4. Analytic solution of LBE for the incompressible Poiseuille flow

It is instructive to show the analytic solutions of the LBE given by Eq. (7) for the *incompressible* Poiseuille flow in 2D. The setup is the following. The channel height is H in the spanwise direction y with N_y grid points, i.e., $j = 1, 2, \ldots, N_y$. A constant body force is applied in the x direction on all fluid nodes. Since we use periodic boundary conditions in the streamwise direction, the channel length L is an irrelevant parameter for the time being. Two horizontal solid walls are placed somewhere below $j = 1$ and above $j = N_y$. The precise wall locations will be determined analytically, as we shall demonstrate next. Because the nonlinear advection term $\boldsymbol{u}\cdot\nabla\boldsymbol{u}$ vanishes for the *incompressible* Poiseuille flow, therefore the nonlinear terms (in u) in $m_i^{(\mathrm{eq})}$ of Eq. (10c) can be neglected. In addition, we assume ρ is a constant. Then a steady state solution can be obtained [33]:

$$\rho u(j) = \frac{4}{N_y^2}\left(j - \frac{1}{2}\right)\left(N_y + \frac{1}{2} - j\right)\rho U_{\max} - \frac{1}{2}\rho G\delta_t + \rho U_s, \quad j \in \{1, 2, \ldots, N_y\}, \tag{14}$$

where $U_{\max} = GH^2/8v$ is the maximum streamwise velocity, $G := |\nabla p|/\rho$ is the acceleration due to a constant pressure gradient, and the term U_s is a constant "slip velocity" which shall discussed in detail later. The term $G\delta_t/2$ suggests that u should be measured after adding $G\delta_t/2$ [34]. This is also consistent with the second-order Chapman–Enskog analysis [28]. Eq. (14) clearly indicates that the channel width ıH is $N_y\delta_x$ and the boundary conditions must be satisfied at $j = 1/2$ and $j = N_y + 1/2$. Only when the desired boundary conditions are satisfied exactly at $j = 1/2$ and $j = N_y + 1/2$, we will have $H = N_y\delta_x$. Eq. (14) can be written in a dimensionless form,

$$\tilde{u}(\tilde{y}) = 4\tilde{y}(1 - \tilde{y}) + \tilde{U}_s, \tag{15}$$

where $\tilde{u} := (u + G\delta_t/2)/U_{\max}$, $\tilde{U}_s := U_s/U_{\max}$, and $\tilde{y} := (j - 1/2)/N_y$. We will next analyze U_s, which depends on the boundary conditions at solid walls and the relaxation rates $\{s_i\}$.

4.1. Bounce-back boundary conditions

The bounce-back boundary conditions mimic the particle-wall interaction that, when a particle collides with a solid wall, its momentum is reversed. Therefore, the bounce-back boundary conditions at a node next to a solid boundary are:

$$f_i(t_{n+1}) = f_i^*(t_n), \tag{16}$$

where $\boldsymbol{c}_i := -\boldsymbol{c}_i$ is a velocity pointing to the solid boundary, and f_i^* denotes a post-collision distribution function. Therefore, adjacent to the channel walls at $j = 1$ and $j = N_y$, we have, respectively:

$$f_{2,5,6}(j = 1, t_{n+1}) = f_{4,7,8}^*(j = 1, t_n), \tag{17a}$$

$$f_{4,7,8}(j = N_y, t_{n+1}) = f_{2,5,6}^*(j = N_y, t_n). \tag{17b}$$

With the bounce-back boundary conditions, we find

$$U_s^{\mathrm{B}} = \frac{1}{4}\left(\frac{8}{s_q} - \frac{8 - s_v}{2 - s_v}\right)G\delta_t, \tag{18}$$

where s_v is the relaxation rate for the stresses, which determines the shear viscosity v given by Eq. (12a), and $s_q = s_5 = s_7$ is the relaxation rate for the moments related to the energy fluxes.

Therefore, U_s^{B} vanishes if and only if s_q and s_v satisfy the following relationship:

$$s_q = \frac{8(2 - s_v)}{(8 - s_v)}, \tag{19}$$

which was first reported by Ginzburg and Adler [28].

Some clarifications are in order concerning the closure relationship (19). First, it is important to note that the relationship (19) of $s_q(s_v)$ to satisfy the Dirichlet boundary condition $U_s^B = 0$ at the location $\delta_x/2$ beyond the last fluid nodes adjacent to a boundary is valid only when the boundary is parallel to the lattice axis. If the boundary is parallel to the diagonals, a similar closed relationship between $s_q(s_v)$ can be obtained [28]:

$$s_q = \frac{4(2 - s_v)}{(4 + s_v)}. \tag{20}$$

It should be stressed that the reason for the closed relationship $s_q = s_q(s_v)$ to exist is that the exact analytic solution of the lattice Boltzmann equation exists for the *incompressible* Poiseuille flow with the boundaries along a lattice line or a diagonal line [28].

However, when the angle between a straight boundary and a lattice axis is arbitrary between 0 and $\pi/4$, then the analytic solution for the Poiseuille flow does not exist for the LBE with bounce-back boundary conditions [28,30], hence no closed relationship of $s_q(s_v)$ can satisfy the imposed Dirichlet boundary conditions exactly. In other words, the bounce-back boundary conditions are inadequate to attain the Dirichlet boundary conditions precisely at a specified location [35]. In this case, one must use interpolations at boundaries [31,36] or the multi-reflection (MR) boundary conditions involving distribution functions at multiple locations near the boundary [23,30]. With the multi-reflection boundary conditions [23,30], both MRT and LBGK models admit the analytic solution for the Stokes-Poiseuille flow, in which the nonlinear terms of equilibria in terms of $\boldsymbol{u}$ have been neglected, with its boundaries arbitrarily oriented with respect to the underlying lattice. It should be stressed that multiple relaxation times are required for the LBE to admit the analytic solution for the Stokes-Poiseuille flow with the bounce-back boundary conditions in the cases where the boundaries are either aligned with a lattice line or a diagonal line [23].

Secondly, in order to obtain Eq. (19), one must assume a constant pressure gradient ∇p along the channel provided that the constant ∇p is modeled correctly [30]. In addition, one must also use the incompressible approximation of the LBE model [37] in which a constant density ρ_0 instead of a variable ρ is used to compute the velocity $\boldsymbol{u}$, i.e., $\boldsymbol{u} = \sum_i \boldsymbol{c}_i f_i/\rho_0$, and the nonlinear terms in the equilibria of Eq. (10c). All the analytic results discussed in this section are obtained with the incompressible approximation.

Finally, we must emphasize the relevance of the analytic solution for the *incompressible* Poiseuille flow to the *compressible* pressure-driven microchannel flow. However, regardless of the physical nature of the flow (compressible vs. incompressible), hydrodynamic boundary conditions must be realized accurately. In particular, the analytic solution illustrates that the fluid–solid boundary conditions are viscosity-dependent for the LBGK model with bounce-back boundary conditions, which is unphysical. The solution of the incompressible Poiseuille flow is the dominant leading-order solution for the compressible pressure-driven microchannel flow in terms of the small parameter $\varepsilon := H/L$, as indicated by Eq. (4a). In Section 4.5 we will show unequivocally that it is *impossible* for the lattice BGK model with the bounce-back boundary conditions to accurately realize the viscosity-independent Dirichlet boundary conditions for the incompressible Poiseuille flow [28,30], and the MRT-LBE model must be used if one wishes to use the bounce-back scheme or any of its variations, which involve strictly local information on a grid. For compressible flows, consistent inlet and outlet boundary conditions are crucial, and this will be discussed in Section 5.

4.2. Diffusive boundary conditions

The diffusive boundary conditions for the LBE can be directly derived from its continuous counterpart in kinetic theory, i.e., Maxwell's boundary conditions [38,39], and are given by:

$$f_i = \frac{\sum_{\boldsymbol{c}_k} |\boldsymbol{c}_k \cdot \hat{\boldsymbol{n}}| f_k^*}{\sum_{\boldsymbol{c}_k} |\boldsymbol{c}_k \cdot \hat{\boldsymbol{n}}| f_k^{(\mathrm{eq})}(\rho_w, \boldsymbol{u}_w)} f_i^{(\mathrm{eq})}(\rho_w, \boldsymbol{u}_w) := f_i^D, \quad \boldsymbol{c}_k \cdot \hat{\boldsymbol{n}} < 0, \tag{21}$$

where $\hat{\boldsymbol{n}}$ is the unit vector out normal to the wall, $\boldsymbol{c}_k$'s are *incidental* velocities defined by $\boldsymbol{c}_k \cdot \hat{\boldsymbol{n}} < 0$, and ρ_w and $\boldsymbol{u}_w$ are density and velocity at the wall, respectively. The distributions f_k^* in Eq. (21) are the post-collision values. Also, the same ρ_w and $\boldsymbol{u}_w$ are used in the equilibria $f_k^{(\mathrm{eq})}$ and $f_i^{(\mathrm{eq})}$ in Eq. (21), hence the ratio $f_k^{(\mathrm{eq})}/\sum_k |\boldsymbol{c}_k \cdot \hat{\boldsymbol{n}}| f_k^{(\mathrm{eq})}$ is a constant independent of ρ_w and $\boldsymbol{u}_w$ for a flat wall parallel to a lattice line or diagonal. Therefore, at the lower wall for instance, we have

$$f_2(t_{n+1}) = 4f_5(t_{n+1}) = 4f_6(t_{n+1}) = \frac{2}{3}[f_4^*(t_n) + f_7^*(t_n) + f_8^*(t_n)]. \tag{22}$$

Then the velocity at the boundary U_s is given by:

$$U_s^D = U_s^B + \frac{3}{2} N_y G \delta_t = U_s^B + \frac{3}{2} \frac{HG}{c}, \tag{23}$$

where $c := \delta_x/\delta_t$.

4.3. Diffusive bounce-back boundary conditions

If we combine the diffusive and the bounce-back boundary conditions:

$$f_i(t_{n+1}) = \beta f_i^*(t_n) + (1-\beta) f_i^{\mathrm{D}}(t_n), \qquad \beta \in [0,1], \tag{24}$$

where $f_i^{\mathrm{D}}(t_n)$ is given by Eq. (21), then the boundary velocity becomes:

$$U_s^{\mathrm{BD}} = U_s^{\mathrm{B}} + \frac{3}{2}\frac{(1-\beta)}{(1+\beta)} N_y G \delta_t = U_s^{\mathrm{B}} + \frac{3}{2}\frac{(1-\beta)}{(1+\beta)}\frac{HG}{c}. \tag{25}$$

With $\beta = 0$ or 1, the above formula reduces to Eq. (23) or Eq. (18), respectively, corresponding to the pure diffusive or bounce-back boundary conditions.

4.4. Specular reflective bounce-back boundary conditions

For a particle colliding with a solid wall, the specular reflective boundary conditions reverse its momentum perpendicular to the wall, and maintain its momentum tangential to the wall. The combination of specular reflective and the bounce-back boundary conditions is implemented as the following:

$$f_{5,6}(j=1, t_{n+1}) = \beta f_{7,8}^*(j=1, t_n) + (1-\beta) f_{8,7}^*(j=1, t_n). \tag{26}$$

With the above boundary conditions, the boundary velocity is

$$U_s^{\mathrm{BR}} = U_s^{\mathrm{B}} + \frac{3}{2}\frac{(1-\beta)}{\beta} N_y G \delta_t = U_s^{\mathrm{B}} + \frac{3}{2}\frac{(1-\beta)}{\beta}\frac{HG}{c}. \tag{27}$$

4.5. Defects in the lattice BGK models with the bounce-back boundary conditions

For the lattice BGK equation, there is only one relaxation rate: $s_i = 1/\tau$. Therefore, with the bounce-back boundary conditions, the boundary velocity of Eq. (18) becomes:

$$U_s^{\mathrm{BGK}} = \frac{(16\tau^2 - 16\tau + 1)}{4(2\tau - 1)} G\delta_t = \frac{48v^2 - 1}{8v} G\delta_t, \tag{28}$$

where $v = (\tau - 1/2)/3$ is the dimensionless viscosity, normalized by $\delta_x = \delta_t = 1$. Therefore, for the lattice BGK equation with the bounce-back boundary conditions, U_s^{BGK} does not vanish unless $v^2 = 1/48$. The results of U_s for the diffusive, the diffusive bounce-back, and the reflective bounce-back boundary conditions remain the same, with U_s^{B} replaced by U_s^{BGK}. The results also hold for the lattice BGK models in 3D.

For the 2D channel flow with a constant pressure gradient, the total mass-flow rate for the LBGK models with the diffusive bounce-back boundary conditions can be deduced from Eq. (14):

$$\frac{\dot{m}_{\mathrm{BGK}}}{\dot{m}_0} = 1 + \left[\frac{8}{\mathfrak{A}^2} Kn^2 + \frac{1}{\mathfrak{A}}\left(6\frac{(1-\beta)}{(1+\beta)} - \frac{10}{N_y}\right) Kn - 3\frac{(1-\beta)}{(1+\beta)}\frac{1}{N_y}\right]\delta_t + \frac{(\delta_t + 3)}{2N_y^2}, \tag{29}$$

where $\dot{m}_0 := 2\rho U_{\max} N_y/3$ and $Kn = \mathfrak{A}\tau/N_y$ with a parameter $\mathfrak{A} > 0$ is assumed [6,7,20]. The above result is obtained by summing Eq. (14) over j with U_s given by Eq. (25). A similar result can be obtained by assuming $Kn = \mathfrak{B}v/N_y$, where $\mathfrak{B} > 0$ is a parameter [5,8,9,11,12,10,13–19]. Thus, with two adjustable parameters, τ and N_y, in addition to $\mathfrak{A}$ (or $\mathfrak{B}$), the above formula is used to fit the flow rate with the Knudsen minimum, and the asymptotic behaviors in both $Kn = 0$ and $Kn \to \infty$ [15,17,18]. It must be noted once again that the flow rate $\dot{m}_{\mathrm{BGK}}$ given above is grid-resolution dependent, that is, the resolution N_y is used as a tuning parameter in the simulation. The above result summarizes the essence of the majority, if not all, of the previous results of the LBGK models with the bounce-back boundary boundary conditions for microflows [5–20].

The above result of U_s given by Eq. (28) has an important consequence – it clearly demonstrates the deficiency of the LBGK model with the bounce-back boundary conditions to predict the flow in microchannel by using U_s as the "slip velocity" [25]. First and foremost, the LBGK model with the bounce-back scheme of this kind cannot resolve the Knudsen layer, regardless how fine the grid is. Furthermore, the "slip velocity" U_s at the wall depends on the grid number N_y [40,33], regardless where the wall locations are set. The above result clearly indicates that: (a) the velocity U_s is a numerical artifact of the LBGK model with the bounce-back boundary conditions, rather than a physical effect, because of its dependence on the grid-resolution N_y; (b) when the wall location is fixed, the "slip velocity" U_s exists in general even if the no-slip bounce-back boundary conditions are used; and (c) the so-called "slip velocity" U_s is viscosity-dependent as a consequence of the viscosity-dependence of the bounce-back type boundary conditions with the LBGK models, which is unphysical. By manipulating the bounce-back scheme, one can set $U_s = 0$ or eliminate the term related to N_y in Eq. (28) with a fixed value of τ. However, one cannot eliminate v-dependence in U_s in LBGK models with bounce-back boundary conditions for arbitrary value of τ [33].

Clearly, the approach using the LBGK model with the bounce-back boundary conditions described above cannot possibly yield correct flow fields in the microchannel. And no comprehensive study has been carried out to compare the LBE with more matured techniques such as DSMC for micro-flow simulations. Only recently a study has shown that, when compared with the DSMC results, the lattice BGK results for the microchannel flow is *qualitatively* incorrect when $Kn \geqslant 0.2$ [26]. To overcome these shortcomings in the LBGK equation, we have to use the collision model with multiple relaxation times (MRT) [27–29], as we will show in what follows.

5. Boundary conditions in LBE simulations

Correct boundary conditions are crucially important in the LBE simulations of microchannel flows. Two types of boundary conditions must be dealt with: (a) the boundary conditions at the walls and (b) pressure boundary conditions at the inlet and the outlet. In our simulations, the system size is $(N_x+2)\times(N_y+2)$, i.e., $i=0,1,\ldots,N_x,N_x+1$, and $j=0,1,\ldots,N_y,N_y+1$. The fluid nodes are $1\leqslant i\leqslant N_x$ and $1\leqslant j\leqslant N_y$. The extra nodes beyond the fluid region are used to store data before advection.

We use the diffusive bounce-back boundary conditions of Eq. (24) at the wall, in which the probability β has to be determined. We can rewrite u and v in dimensional form:

$$u(\tilde{x},\tilde{y}) = U_{\max}\left[(1-4\tilde{y}^2)+4\frac{Kn}{\tilde{p}}\right], \tag{30a}$$

$$v(\tilde{x},\tilde{y}) = V_{\max}\left[\left(1-\frac{4}{3}\tilde{y}^2\right)+4Kn\frac{2\tilde{p}''}{(\tilde{p}^2)''}\right]\tilde{y}, \tag{30b}$$

where $U_{\max}=H^2|p'|/8\mu$, $V_{\max}=H^3(p^2)''/16\mu p$, and we assume $\sigma=1$. The $\tilde{x}$-dependence of u and v is through p and its derivatives. Then, combining Eqs. (30a) and (25), the first-order slip velocity is:

$$U_s = 4\frac{Kn}{\tilde{p}}U_{\max} = \frac{Kn}{\tilde{p}}\frac{|\nabla p|H^2}{2\rho\nu} = \frac{3}{2}\frac{(1-\beta)}{(1+\beta)}\frac{|\nabla p|}{\rho}\frac{H}{c}, \tag{31}$$

where Eq. (25) with $U_s^B=0$ and $H=N_y\delta_x$ and $c:=\delta_x/\delta_t$ has been used. This leads to

$$\beta = \frac{3\mu - KnHc\bar{\rho}_{\text{out}}}{3\mu + KnHc\bar{\rho}_{\text{out}}}. \tag{32}$$

It is clear that β is a constant because μ is a constant for the first-order slip model [3].

The inlet and the outlet pressure boundary conditions are crucial for the simulations. The constant pressure boundary conditions would not work here because the inlet and outlet pressure conditions must be consistent with the flow field inside the channel. We use extrapolated boundary conditions at both ends of the channel. At the inlet ($i=0$) and the outlet ($i=N_x+1$) ghost nodes, the unknown distribution functions, which will advect from boundaries into the channel, are computed from interior fluid nodes along the streamwise direction before advection according to the following extrapolation formulas:

$$f_k(0,j) = 2f_k(1,j) - f_k(2,j), \quad k=\{1,5,8\}, \tag{33a}$$

$$f_k(N_x+1,j) = 2f_k(N_x,j) - f_k(N_x-1,j), \quad k=\{3,6,7\}, \tag{33b}$$

where $j\in\{1,2,\ldots,N_y\}$. After the extrapolation, the unknown distribution functions are propagated to adjacent fluid nodes. The densities at both the inlet ($i=1$) and the outlet ($i=N_x$) can be computed now. Then the densities at the inlet ($i=1$) and outlet ($i=N_x$) are renormalized along the spanwise direction (y) so that their *averaged* values are equal to $\bar{\rho}_{\text{in}}$ and $\bar{\rho}_{\text{out}}$ stipulated by the pressure boundary conditions, respectively. The renormalized values of $\rho_{\text{in}}(j)$ and $\rho_{\text{out}}(j)$ are used in the equilibria to carry out the ensuing collision step. This procedure ensures that on *average* the pressure boundary conditions are satisfied, and more importantly, the pressure profiles at both the inlet and the outlet, which are *not* constant along spanwise direction, are consist with flow field inside the channel. We also note that the pressure boundary conditions used here do not lead to observable "boundary layers" at the boundaries.

6. Numerical results

In what follows, we will demonstrate that the lattice Boltzmann equation with the MRT collision model can indeed simulate microchannel flow with finite Knudsen number effects. The boundary conditions described in the previous section are used in the simulations. The values of the relaxation rates are: $s_i=s_\nu=1/\tau$ for $i\neq 5$ and 7, and $s_5=s_7=s_q$, where s_ν is chosen to keep μ constant and s_q is related to s_ν by Eq. (19).

6.1. Convergence study

To conduct a convergence study by varying grid size $N_x\times N_y$, we must maintain constant *Re*, *Ma* and hence *Kn*. This immediately means that the reference velocity $\bar{u}_{\text{out}}$ must be kept constant. It is therefore convenient to use the lattice units that

$\delta_x = \delta_t = 1$. In this convention, the width of the channel $H = \delta_x N_y = N_y$ becomes a variable. Consequently the shear viscosity v also becomes a variable. It follows that the viscosity v can be given in terms of the local Knudsen number $Kn/\tilde{p}$ and N_y:

$$v = \sqrt{\frac{2}{3\pi}}\frac{Kn}{\tilde{p}}N_y. \tag{34}$$

Therefore, with Kn fixed, the viscosity $v = (\tau - 1/2)/3$, and henceforth τ, depend linearly on the mesh size N_y, which creates a difficulty for the lattice BGK model with bounce-back boundary conditions, but not for the MRT-LBE. Obviously, the system with constant Re, Ma, and Kn will *not* converge to the incompressible Navier–Stokes equation for which most LBE models are intended in the limit of $Ma \to 0$.

We conduct a convergence study with the following system: $\rho_{in} = 1.01$ and $\rho_{out} = 1.0$, $\varepsilon = H/L = 1/4$, and compute relative errors of u, v and ρ with 4 different mesh sizes: $N_x \times N_y = 16 \times 4$, 32×8, 64×16, and 128×32. Accordingly, $\mu = 1/16$, $1/8$, $1/4$, and $1/2$. The relative error is computed with L^2-norm:

$$E_2(u) = \sqrt{\frac{\sum_j [u_\delta(r_j) - u(r_j)]^2}{\sum_j u(r_j)^2}}, \tag{35}$$

where u_δ and u are the numerical and analytic (Eqs. (4a)) solutions, respectively. Fig. 1 shows the results of the convergence study. The least-square fitted slopes of $E_2(u)$, $E_2(v)$ and $E_2(\rho)$ are 0.97, 1.07 and 1.13, respectively, indicating convergence to Eq. (4a).

It is interesting to note that the second-order convergence of the LBE in space can be obtained through asymptotic analysis [41] in the following limit with diffusive scaling for incompressible flows [42,43]: $\delta_x = \delta_t^2 \sim \epsilon^2$, $Ma \sim \epsilon$, and $\epsilon \to 0$. However, we are dealing with compressible flows here. The limit we are taking is: $\delta_x = \delta_t \sim \epsilon$, $Ma =$ constant, and $\epsilon \to 0$. This may explain the first-order convergence observed in Fig. 1. However, a definitive analysis for the convergence behavior of the compressible LBE models remains to be investigated.

6.2. Microchannel flow in the slip flow regime

We now simulate flow through a long microchannel. The system size is $N_x \times N_y = 1100 \times 11$, thus $\varepsilon = H/L = 1/100$. The averaged outlet density is fixed at $\bar{\rho}_{out} = 1.0$.

We choose three values for the Knudsen number: $Kn = 0.0194$, 0.194 and 0.388. The values for the averaged inlet density are: $\bar{\rho}_{in} = 1.4$ for $Kn = 0.0194$, and $\bar{\rho}_{in} = 2.0$ for $Kn = 0.194$ and 0.388. We choose these particular values of $\bar{\rho}_{out}/\bar{\rho}_{in}$ and Kn so our results can be compared with those obtained by other methods [26,44]. We compute the velocities u and v, and the deviation of the pressure from the linear profile of the no-slip incompressible Navier–Stokes solution:

$$\delta p(\tilde{x}) = \frac{1}{p_{out}}(p - p_{NS}), \tag{36}$$

where p_{NS} is the linear pressure distribution along the channel center line.

Fig. 2 presents our results of the pressure deviation from the linear distribution along the centerline, the normalized streamwise velocity u/U_{max} and the normalized normal velocity v/V_{max} at the outlet. In all cases, the LBE results agree very well with the results of the compressible Navier–Stokes equation with a slip velocity (Slip-NS), given by Eq. (4a). The largest L_2-normed differences of δp, u/U_{max} and v/V_{max} between the LBE and the slip-NS results at $Kn = 0.388$ are 4.0%, 1.5% and 15.0%, respectively. We note that $V_{max} \sim 10^{-6}$ is four orders of magnitude smaller than U_{max}, and although $\tilde{v}$ is accurately captured by the LBE, its error is much larger than that of $\tilde{u}$. At $Kn = 0.0194$, the flow is in the near continuum or the slip flow regime. In this case, the LBE results agree well with the information-preservation DSMC (IP-DSMC) and the DSMC results of

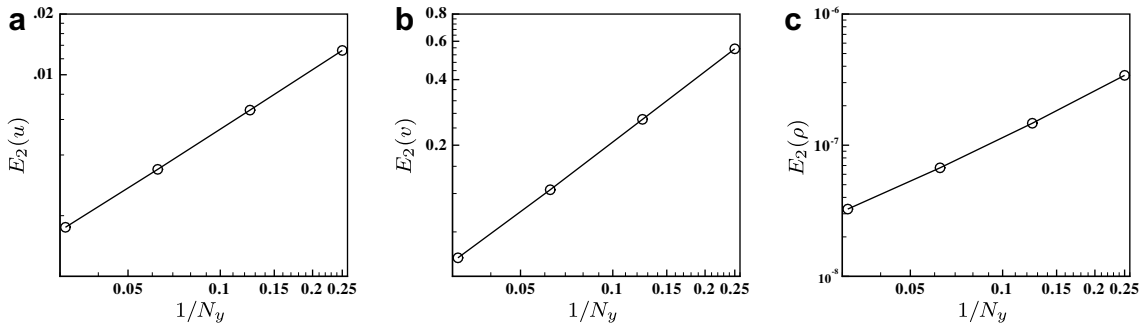

Fig. 1. The errors of the flow fields. (a) The streamwise velocity $E_2(u)$ with a slope of 0.97, (b) the normal velocity $E_2(v)$ of a slope 1.07, and (c) the density $E_2(\rho)$ with a slope of 1.13.

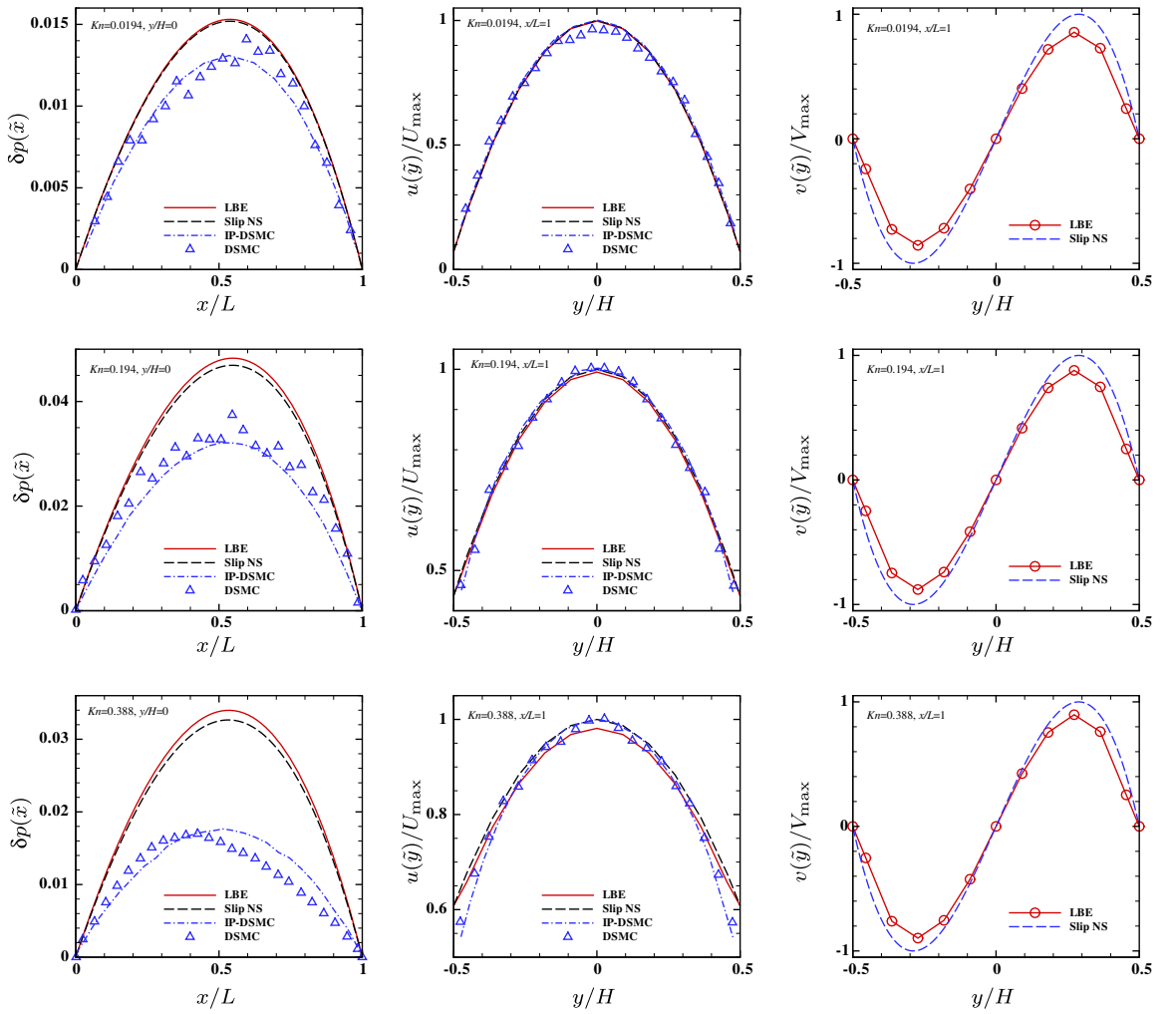

Fig. 2. The LBE results (solid lines) vs. the analytic solutions of the slip Navier–Stokes equation (dashed lines) and the results of IP-DSMC (dash-dotted lines) and DSMC (△). Top: $Kn = 0.0194$; middle: $Kn = 0.194$; and bottom: $Kn = 0.388$. Left: $\delta p(\tilde{x})$ along the channel centerline; Center: $u(\tilde{y})/U_{\max}$ at the outlet $\tilde{x} = 1$; and Right: $v(\tilde{y})/V_{\max}$ at the channel outlet $\tilde{x} = 1$, the circles indicate the grid and boundary locations.

Shen et al. [26]. There is very little difference in the streamwise velocity at the outlet, but the maximum δp obtained by the LBE is about 17% larger than that by IP-DSMC. The difference in maximum δp increases as Kn increases: at $Kn = 0.194$ it is a factor of about 1.5 and at $Kn = 0.388$ a factor of about 2. The difference in $u/U_{\max}$ is relatively small when $Kn = 0.194$, but becomes larger near the wall when $Kn = 0.388$. This is expected because the first-order slip velocity model used here is no longer valid for this Knudsen number. For transitional flows, one must used more sophisticated models, which can include either higher-order velocity derivatives [2] or more than one accommodation coefficient, such as Cercignani-Lampis model [45]. We note that these more sophisticated models can be readily integrated in the present lattice Boltzmann model.

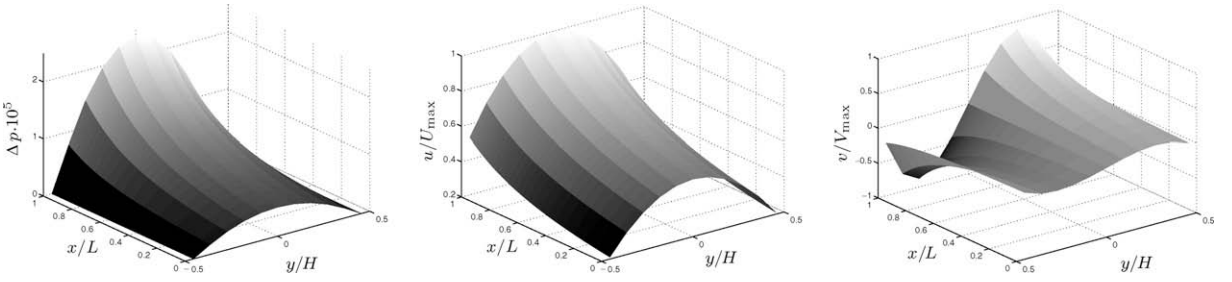

Fig. 3. Flow fields on $\tilde{x}$-$\tilde{y}$ plane, $Kn = 0.194$. Left to right: $\Delta p \cdot 10^5$, $u/U_{\max}$ and $v/V_{\max}$.

Fig. 3 illustrates the two-dimensional nature of the flow. The flow fields on x-y plane with $Kn = 0.194$ are shown as 3D plots. The 2D effect in δp is a consequence of the non-zero normal velocity v, therefore it is of order of v, which is about five orders of magnitude smaller than p. We therefore compute $\Delta p := [\delta p(\tilde{x}, \tilde{y}) - \delta p(\tilde{x}, 0)]$ and magnify Δp by a factor of 10^5 in the figure. Clearly, the flow fields are all two-dimensional. We notice that Δp and $u/U_{\max}$ are similar in Fig. 3, due to the way Δp is computed. The main feature of δp and u should be (and is) different: along the centerline, the former is concave, as shown in Fig. 2, whereas the latter is convex, as shown in Fig. 3.

7. Conclusions

In this work we implement the athermal MRT-LBE with a first-order slip velocity model and demonstrate that the LBE method can be used to simulate gaseous flow through a long microchannel in the slip flow regime. The LBE results agree well with the slip Navier–Stokes, DSMC, and IP-DSMC results in the slip flow regime. While the LBE and slip Navier–Stokes results agree well with each other in the transition-flow regime, they deviate significantly from the DSMC results, as expected.

We would like to point out that the errors in the previous results obtained by using the LBGK model with the bounce-back boundary conditions, as criticized by Shen et al. [26], are mainly due to two causes: the inaccuracy of the bounce-back boundary conditions coupled with the LBGK model and the inconsistent pressure boundary conditions. We show that, for the Poiseuille flow in a long microchannel with boundaries aligned with a lattice axis, certain defects of the LBGK model coupled with the bounce-back boundary conditions can be overcome by the MRT-LBE model, and the pressure boundary conditions consistent with the microchannel flow can be implemented in the LBE method. With the MRT-LBE model and consistent boundary conditions, the MRT-LBE results converge to the compressible NS equations with slip velocity boundary conditions.

The fundamental deficiency of the LBGK model is that, with only one parameter τ, it has no freedom to adjust higher-order discretization errors in bulk or due to boundary conditions, as explicitly shown by Ginzburg for the Brinkman flow [46]. The critics of the MRT-LBE method often insist that the LBGK model is simple and therefore efficient. This is not true. The MRT-LBE models with only two relaxation times (TRT) [30,46] is just as efficient as the corresponding LBGK models with an equal number of velocities, and the TRT-LBE models with the bounce-back boundary conditions can correctly realize the Dirichlet boundary conditions for the Navier–Stokes flows, while the LBGK model with the bounce-back boundary conditions cannot do so, as we have shown in this work.

The present work only deals with the Poiseuille flow with its boundaries aligned with a lattice axis. For flows with complex boundary geometries, alternative boundary conditions that are more accurate than the bounce-back ones must be used [31,36,23,24,30]. The effectiveness of these alternative boundary conditions applied to microflows has yet to be investigated and these schemes deserve further study. In addition, to fully understand the effectiveness of the LBE models for gaseous microflows, one needs to investigate higher-order terms in the Chapman–Enskog expansion [46] for the compressible LBE models with significant density variations. These subjects shall be considered in our future studies.

Finally, we would like to point out that, with slip velocity models, such as Eq. (3) or other more sophisticated higher-order models, the LBE model *cannot* resolve the Knudsen layer. Within the Knudsen layer, the viscosity is not a constant, to say the least. To correctly model microchannel flow with large Kn, one needs to adequately model the effective mean free path as a function of, e.g., the local Knudsen number, as shown by Guo et al. [44]. This and other issues will be left for future research.

Acknowledgments

The authors are indebted to Dr. Z.L. Guo for providing the DSMC and IP-DSMC data of Shen et al. [26] and helpful discussions. LSL is grateful to Dr. I. Ginzburg for many constructive discussions and suggestions. FV would like to acknowledge the support from the Research Foundation-Flanders (FWO-Vlaanderen). LSL would like to acknowledge the support from the National Science Foundation of the US through the Grants CBET-0500213 and DMS-0807983, and NASA Langley Research Center through a C&I grant via the NIA cooperation agreement Grant NCC-1-02043.

References

[1] C.M. Ho, Y.C. Tai, Micro-electro-mechanical-systems (MEMS) and fluid flows, Annu. Rev. Fluid Mech. 30 (1998) 579–612.
[2] G. Em Karniadakis, A. Beskok, N. Aluru, Microflows: Fundamentals and Simulation, Springer, New York, 2005.
[3] E.B. Arkilic, M.A. Schmidt, K.S. Breuer, Gaseous slip flow in long microchannels, J. Microelectromechan. Syst. 6 (2) (1997) 167–178.
[4] M. Gad-el-Hak, The fluid mechanics of microdevices, J. Fluids Eng. 121 (1999) 5–33.
[5] X.B. Nie, G.D. Doolen, S.Y. Chen, Lattice-Boltzmann simulations of fluid flows in MEMS, J. Stat. Phys. 107 (1–2) (2002) 279–289.
[6] C.Y. Lim, C. Shu, X.D. Niu, Y.T. Chew, Application of lattice Boltzmann method to simulate microchannel flows, Phys. Fluids 14 (7) (2002) 2299–2308.
[7] X.D. Niu, C. Shu, Y.T. Chew, A lattice Boltzmann BGK model for simulation of micro flows, Europhys. Lett. 67 (4) (2004) 600–606.
[8] G.H. Tang, W.Q. Tao, Y.L. He, Lattice Boltzmann method for gaseous microflows using kinetic theory boundary conditions, Phys. Fluids 17 (2005) 058101.
[9] T. Lee, C.-L. Lin, Rarefaction and compressibility effects of the lattice Boltzmann equation method in a gas microchannel, Phys. Rev. E 71 (2005) 046706.
[10] A. Agrawal, L. Djenidi, R.A. Antonia, Simulation of gas flow in microchannels with a sudden expansion or contraction, J. Fluid Mech. 530 (2005) 135–144.
[11] Y.H. Zhang, R.S. Qin, Y.H. Sun, R.W. Barber, D.R. Emerson, Gas flow in microchannels – a lattice Boltzmann approach, J. Stat. Phys. 121 (1/2) (2005) 257–267.

[12] Y.H. Zhang, R. Qin, D.R. Emerson, Lattice Boltzmann simulation of rarefied gas flows in microchannels, Phys. Rev. E 71 (2005) 047702.
[13] V. Sofonea, R.F. Sekerka, Boundary conditions for the upwind finite difference lattice Boltzmann model: evidence of slip velocity in micro-channel flow, J. Comput. Phys. 207 (2005) 639–659.
[14] M. Sbragaglia, S. Succi, Analytical calculation of slip flow in lattice Boltzmann models with kinetic boundary conditions, Phys. Fluids 17 (2005) 093602.
[15] S. Ansumali, I.V. Karlin, Consistent lattice Boltzmann method, Phys. Rev. Lett. 95 (26) (2005) 260605.
[16] Y.-H. Zhang, X.-J. Gu, R. Barber, D.R. Emerson, Capturing Knudsen layer phenomena using a lattice Boltzmann model, Phys. Rev. E 74 (2006) 046704.
[17] S. Ansumali, I.V. Karlin, C.E. Frouzakis, K.E. Boulouchos, Entropic lattice Boltzmann method for microflows, Physica A 359 (2006) 289–305.
[18] Y. Zhou, R. Zhang, I. Staroselsky, H. Chen, W.T. Kim, M.S. Jhon, Simulation of micro- and nano-scale flows via the lattice Boltzmann method, Physica A 362 (1) (2006) 68–77.
[19] R. Benzi, L. Biferale, M. Sbragaglia, S. Succi, F. Toshi, Mesoscopic modelling of heterogeneous boundary conditions for microchannel flows, J. Fluid Mech. 548 (2006) 257–280.
[20] S. Ansumali, I.V. Karlin, S. Arcidiacono, A. Abbas, N.I. Prsianakis, Hydrodynamics beyond Navier–Stokes: exact solution to the lattice Boltzmann hierarchy, Phys. Rev. Lett. 98 (12) (2007) 124502.
[21] H. Chen, S. Chen, W.H. Matthaeus, Recovery of the Navier–Stokes equations using a lattice-gas Boltzmann method, Phys. Rev. A 45 (8) (1992) R5339–R5342.
[22] Y.H. Qian, D. d'Humières, P. Lallemand, Lattice BGK models for Navier–Stokes equation, Europhys. Lett. 17 (1992) 479–484.
[23] I. Ginzburg, D. d'Humières, Multireflection boundary conditions for lattice Boltzmann models, Phys. Rev. E 68 (2003) 066614.
[24] C. Pan, L.-S. Luo, C.T. Miller, An evaluation of lattice Boltzmann schemes for porous medium flow simulation, Comput. Fluids 35 (8/9) (2006) 898–909.
[25] L.-S. Luo, Comment on discrete Boltzmann equation for microfluidics, Phys. Rev. Lett. 92 (13) (2004) 139401.
[26] C. Shen, D.B. Tian, C. Xie, J. Fan, Examination of the LBM in simulation of microchannel flow in transitional regime, Microscale Thermophys. Eng. 8 (4) (2004) 423–432.
[27] D. d'Humières, Generalized lattice-Boltzmann equations, in: B.D. Shizgal, D.P. Weaver (Eds.), Rarified Gas Dynamics: Theory and Simulations, vol. 159 of Prog. Astro. Aero, AIAA, 1992, pp. 450–458.
[28] I. Ginzbourg, P.M. Adler, Boundary flow condition analysis for the three-dimensional lattice Boltzmann model, J. Phys. II 4 (191) (1994) 191–214.
[29] P. Lallemand, L.-S. Luo, Theory of the lattice Boltzmann method: dispersion, dissipation, isotropy, Galilean invariance and stability, Phys. Rev. E 61 (6) (2000) 6546–6562.
[30] I. Ginzburg, F. Verhaeghe, D. d'Humières, Study of simple hydrodynamic solutions with the two-relaxation-times lattice Boltzmann scheme, Comm. Comput. Phys. 3 (2008) 519–581.
[31] M. Bouzidi, M. Firdaouss, P. Lallemand, Momentum transfer of Boltzmann-lattice fluid with boundaries, Phys. Fluids 13 (11) (2001) 3452–3459.
[32] A. Beskok, G. Em Karniadakis, W. Trimmer, Rarefaction and compressibility effects in gas microflows, Trans. ASME 118 (1996) 448–456.
[33] X. He, Q. Zou, L.-S. Luo, M. Dembo, Analytic solution of simple flows and analysis of nonslip boundary conditions for the lattice Boltzmann BGK model, J. Stat. Phys. 87 (1/2) (1997) 115–136.
[34] P. Lallemand, L.-S. Luo, Theory of the lattice Boltzmann method: acoustic and thermal properties in two and three dimensions, Phys. Rev. E 68 (3) (2003) 036706.
[35] I. Ginzbourg, D. d'Humières, Local second-order boundary method for lattice Boltzmann models, J. Stat. Phys. 84 (5/6) (1996) 927–971.
[36] P. Lallemand, L.-S. Luo, Lattice Boltzmann method for moving boundaries, J. Comput. Phys. 184 (2) (2003) 406–421.
[37] X. He, L.-S. Luo, Lattice Boltzmann model for the incompressible Navier–Stokes equation, J. Stat. Phys. 88 (3/4) (1997) 927–944.
[38] C. Cercignani, The Boltzmann Equation and Its Applications, Springer, New York, 1988.
[39] S. Harris, An Introduction to the Theory of the Boltzmann Equation, Dover, Mineola, NY, 2004.
[40] L.-S. Luo, Analytic solutions of linearized lattice Boltzmann equation, J. Stat. Phys 88 (3/4) (1997) 913–926.
[41] M. Junk, A. Klar, L.-S. Luo, Asymptotic analysis of the lattice Boltzmann equation, J. Comput. Phys. 210 (2) (2005) 676–704.
[42] Z. Yang, Analysis of lattice Boltzmann boundary conditions, PhD Thesis, Universität Kanstanz, 2007.
[43] M. Junk, Z. Yang. Convergence of lattice Boltzmann methods for Navier–Stokes flows in periodic and bounded domains, Numerische Mathematik., in press.
[44] Z.L. Guo, T.S. Zhao, Y. Shi, Physical symmetry, spatial accuracy, and relaxation time of the lattice Boltzmann equation for micro gas flows, J. Appl. Phys. 99 (2006) 074903.
[45] C. Cercignani, Rarefied Gas Dynamics, Cambridge University Press, Cambridge, UK, 2000.
[46] I. Ginzburg, Consistent lattice Boltzmann schemes for the Brinkman model of porous flow and infinite Chapman–Enskog expansion, Phys. Rev. E 3 (6) (2008) 0666704.